# MR1-dependent immune surveillance of the skin contributes to pathogenesis and is a photobiological target of UV light therapy in a mouse model of atopic dermatitis

Karmella Naidoo, Katherine Woods, Christophe Pellefigues, Alissa Cait, David O'Sullivan, Katie Gell, Andrew J Marshall, Regan J Anderson, Yanyan Li, Alfonso Schmidt, et al.

Article type: Original Article: Atopic Dermatitis, Urticaria and Skin Disease

# MR1-dependent immune surveillance of the skin contributes to pathogenesis and is a photobiological target of UV light therapy in a mouse model of atopic dermatitis.

**Manuscript Acceptance Date: 24-May-2021**

Short title: MR1-dependent immune surveillance drives AD

Karmella Naidoo[1], Katherine Woods[1,#], Christophe Pellefigues[1,#], Alissa Cait[1,#], David O'Sullivan[1,5], Katie Gell[1], Andrew J. Marshall[2], Regan J. Anderson[2], Yanyan Li[1,5], Alfonso Schmidt[1], Kef Prasit[1], Johannes U. Mayer[1], Aurelie Gestin[1], Ian F. Hermans[1], Gavin Painter[2], Elizabeth A. Jacobsen[3], Olivier Gasser[1,5,*]

[1]Malaghan Institute of Medical Research, Wellington 6242, New Zealand

[2]Ferrier Research Institute, Victoria University of Wellington, Lower Hutt, New Zealand

[3]Division of Allergy, Asthma and Clinical Immunology, Mayo Clinic Arizona, Scottsdale, Arizona, USA

[5]High-Value Nutrition National Science Challenge, Auckland, New Zealand

[#]Authors contributed equally to this work

[*]Correspondence: Olivier Gasser, Malaghan Institute of Medical Research, Kelburn Parade, Wellington, New Zealand. Email: ogasser@malaghan.org.nz

Word count: 5254

**Acknowledgments:** This work was supported by the New Zealand Health Research Council Independent Research Organization Fund (14/1003), the High-Value Nutrition National Science Challenge, New Zealand, the New Zealand Ministry of Business Innovation and Employment (RTVU1603), Dairy Goat Co-operative Limited, New Zealand and the New Zealand Ministry for Primary Industries as part of the Caprine Innovations NZ (CAPRINZ) Sustainable Food & Fibre Futures programme. We are grateful to the the staff of the Hugh Green Cytometry Core and Biomedical Research Unit at the Malaghan Institute of Medical Research for expert support with flow cytometry and animal husbandry and all colleagues at the Malaghan Institute for insightful discussion and advice. We thank the NIH Tetramer Facility for providing the 5-OP-RU- and 6-FP-loaded MR1 tetramers. The MR1 tetramer technology was developed jointly by Dr. James McCluskey, Dr. Jamie Rossjohn, and Dr. David Fairlie, and the material was produced by the NIH Tetramer Core Facility as permitted to be distributed by the University of Melbourne, Australia. Dr. Naidoo is listed as an inventor on a pending patent protecting the use of MR1 ligands in the context of inflammatory skin diseases. Dr Woods has nothing to disclose. Dr. Pellefigues has nothing to disclose. Dr. Cait has nothing to disclose. Dr. O'Sullivan has nothing to disclose. Ms. Gell has nothing to disclose. Dr. Marshall reports grants from Ministry of Business Innovation and Employment during the conduct of the study. Dr. Anderson reports grants from Ministry of Business Innovation and Employment during the conduct of the study. Ms. Li has nothing to disclose. A.J. Schmidt has nothing to disclose. Dr. Prasit has nothing to disclose. Dr. Mayer has nothing to disclose. Dr. Gestin has nothing to disclose. IH declares no conflicts of interest. Dr. Painter reports grants from NZ Ministry of Business Innovation and Employment, grants from the NZ Health Research Council, during the conduct of the study. Dr. Jacobsen has nothing to disclose. Dr. Gasser is listed as an inventor on a pending patent protecting the use of MR1 ligands in the context of inflammatory skin diseases.

**Abstract**

**Background:** Mucosal-associated invariant T (MAIT) cells are unconventional T cells which recognize microbial metabolites presented by the major histocompatibility complex class I-related molecule MR1. Although MAIT cells have been shown to reside in human and murine skin, their contribution to atopic dermatitis (AD), an inflammatory skin disease associated with barrier dysfunction and microbial translocation, has not yet been determined.

**Methods:** Genetic deletion of MR1 and topical treatment with inhibitory MR1 ligands, which result in the absence and functional inhibition of MAIT cells, respectively, were used to investigate the role of MR1-dependent immune surveillance in a MC903-driven murine model of AD.

**Results:** The absence or inhibition of MR1 arrested AD disease progression through the blockade of both eosinophil activation and recruitment of IL-4 and IL-13 producing cells. In addition, the therapeutic efficacy of phototherapy against MC903-driven AD could be increased with prior application of folate, which photodegrades into the inhibitory MR1 ligand 6-formylpterin.

**Conclusion:** We identified MAIT cells as sentinels and mediators of cutaneous type-2 immunity. Their pathogenic activity can be inhibited by topical application or endogenous generation, via phototherapy, of inhibitory MR1 ligands.

**Keywords:** atopic dermatitis, MR1, MAIT cells, phototherapy

## Introduction

Mucosal-associated invariant T (MAIT) cells are an innate-like T cell subset, which patrol mucosal tissues such as the gut and the lung [1-3]. Their frequency is exceptionally high in humans, where they represent up to 5% of circulating T cells and 50% of liver-resident T cells [4-7]. Canonical MAIT cells express an invariant T cell receptor (TCR) α-chain –Vα7.2 in humans and Vα19 in mice– which recognizes microbial riboflavin metabolites presented by major histocompatibility complex (MHC) related molecule 1 (MR1) [8,9]; both ligand and receptor –i.e. microbial colonization of the host and expression of MR1– are required for peripheral MAIT cell maturation and expansion [10]. Although human MAIT cells have been shown to efficiently lyse bacteria-infected cells *in vitro*, their protective role *in vivo* in the context of animal bacterial infection models is most apparent in genetically modified backgrounds, such as Vα19-transgenic [5] or immunodeficient RAG2-/-γC-/- mice [11,12]. This indicates that MR1-restricted bacterial recognition, in the context of either microbial pathogenesis or commensalism, may have been evolutionarily selected to provide other immunological functions beyond cytotoxicity [13]. This is also suggested by the tissue-specific secretion of homeostatic cytokines by resident MAIT cells (*e.g.* IL-22 in the gastrointestinal mucosa [14]) and the involvement of MAIT cells in infectious as well as non-infectious diseases [15,16].

The presence of MAIT cells in human skin has been reported [17] but their contribution to local disease is currently unknown. Due to the significant role of microbial skin colonization in local homeostasis and disease [18,19], we reasoned that skin resident MAIT cells might represent one of its cellular mediators. In particular, we considered a possible role of MAIT cells in atopic dermatitis (AD; eczema), a common chronic skin disease associated with highly pruritic lesions, loss of skin barrier function and increased host-bacterial crosstalk [20]. Intriguingly, exposure to ultraviolet light, from sunlight or in the context of phototherapy (a second-line treatment for AD [20]), is known to degrade folate in the skin to 6-formylpterin (6-FP) [21,22], which is a reported antagonist of MAIT cells [9,23]. However, the physiological effects of this bioactive photometabolite have not yet been addressed.

Here, we report that genetic deletion of MR1 or functional blockade of MAIT cells, via the use of competitive antagonists of MAIT cell activation (including synthetic 6-FP), results in decreased pathology in a murine model of AD. Mechanistically, the therapeutic efficacy of MAIT cell

antagonists was linked to the repression of skin-infiltrating eosinophil activation and the diminished recruitment of IL-4 and IL-13 producing cells, including basophils and innate lymphoid cells (ILC). We further demonstrate the MR1- and folic acid-dependence of phototherapy-mediated immunosuppression and propose its combination with topical folic acid for therapeutic enhancement.

## Results

### Atopic Dermatitis Pathogenesis is MR1-Dependent

In a clinically relevant MC903-driven model of atopic dermatitis [24], we show that MAIT cell deficiency resulted in significantly decreased disease severity, as assessed by ear thickness (Fig. 1A) and trans-epidermal water loss (TEWL), a surrogate marker of skin barrier function (Fig. 1B) [25]. Histopathological analyses further revealed a marked reduction in both dermal and epidermal (acanthosis) thickening (Fig. 1, C-E). AD induced a significant infiltration of MAIT cells into the diseased skin area (Fig. 1, F and G), and a shift towards higher CD4 co-receptor expression (Fig. 1H). Additional phenotyping of skin-resident MAIT cells showed downregulation of the receptor for thymic stromal lymphopoietin (TSLP), a key mediator of MC903-induced AD [26,27], and signs of cellular activation and tissue residency as indicated by the co-expression of CD69 and CD103 [28] (Fig. 1I). These initial findings led us to hypothesize that MC903-induced pruritus (itch) and concomitant scratching led to physical damage to the skin barrier, bacterial translocation across the skin epithelium and recognition of the bacterial riboflavin metabolites by MAIT cells, resulting in an inflammatory cascade which was successfully blocked in the absence of MR1. Consistent with this hypothesis, topical pretreatment with antibiotics (polymyxin B, bacitracin and neomycin) [29] had a similar effect on ear thickening and TEWL in the MC903 model (Fig. S1, A-C). Importantly, topical antibiotic treatment of MR1-/- mice did not further decrease disease severity, suggesting that both treatment modalities operate *via* the same mode of action. Circulating levels of TSLP were unaffected by the antibiotic treatment (Fig. S1D).

### Antagonistic MR1 Ligands Block Atopic Dermatitis

Next, we examined if a similar disease reduction is achievable by topical application of the previously described MAIT cell antagonists 6-formylpterin (6-FP) and acetyl-6-FP (Ac-6-FP) [9,23]. The prophylactic co-administration of either 6-FP or Ac-6-FP with MC903 resulted in significantly decreased ear thickness and TEWL (Fig. S2, A-D). Histopathology of diseased skin recapitulated the reduced epidermal and dermal thickening observed in MR1-/- mice (Fig. S2, E and F). Therapeutic application of Ac-6-FP from day 9 also arrested disease progression, dose dependently (Fig. S3), with no further improvement observed in MR1-/- mice (Fig. 2, A-D). Similar results were obtained with 6-

FP (Fig. S4) as well as other described antagonistic MR1 ligands [30,31] (Fig. S5). Unexpectedly, therapeutic application of Ac-6-FP not only inhibited tissue pathology but actively promoted tissue repair, as reflected by the upregulation of genes typically associated with extracellular matrix remodeling [32]: *Furin*, *Mmp10* and *Mmp25* (Fig. 2E). Quantitative analyses of ear sections by confocal microscopy further indicated an increased production of vimentin, a cytoskeletal protein crucial for cutaneous wound healing [33], an increase in CD31-expressing endothelial cells [34], indicating neovascularization and angiogenesis, as well as increased keratinocyte proliferation (Ki-67$^+$keratin14$^+$ cells) (Fig. 2, F and G).

**MR1-dependent Immune Surveillance Controls Cutaneous Eosinophil Function and Atopic Effector Mechanisms**

Our previous work indicated that eosinophils are key mediators of AD-driven tissue injury [24]. We therefore determined whether MAIT cells influence eosinophilic recruitment into developing AD lesions. Surprisingly, therapeutic treatment with Ac-6-FP or genetic deletion of MR1 did not reduce the frequency of skin-infiltrating eosinophils, as determined by flow cytometry as well as immunofluorescence (Fig. 3A, C and D and Fig. S6). However, we observed the inability of extravasated eosinophils to attain an activated phenotype in the presence of Ac-6-FP. Homeostatic and activated eosinophils differ phenotypically in a tissue-specific manner [35]. While the biology of cutaneous eosinophils has yet to be fully established, we considered a range of activation markers to characterize the phenotype of skin-infiltrating eosinophils in the context of AD [36,37]. As shown in Fig. 3B, MC903 induced robust eosinophilic activation, as reflected by the significant increase of each of the phenotypic categories considered here: CD69$^+$, CD44$^+$CD69$^+$PDL1$^+$ and CD44$^+$CD62L$^+$ eosinophils. In each case, Ac-6-FP treatment blocked the progression from homeostatic to activated phenotype (Fig. 3B). To further demonstrate the mechanistic link between MAIT cells and eosinophils, we depleted eosinophils (using diphtheria toxin (DT) administration in iPHIL mice [38]) from day 6 of MC903 application and compared the associated disease outcome to the therapeutic effects of Ac-6-FP administration (from day 9), and to their combined impact on disease progression (Fig. 3, F-I). Depletion of eosinophils from day 6 led to significant decreases in ear thickness (Fig. 3, F and G), TEWL (Fig. 3H) as well as epidermal and dermal thickening (Fig. 3I), consistent with what we observed when depleting eosinophils from the first day of treatment [24]. Treatment with Ac-6-FP

resulted in a very similar disease severity, although with slightly improved epidermal and dermal thickening compared to eosinophil depletion alone (Fig. 3, F-I). Importantly, combining eosinophil depletion and MAIT cell antagonism was indistinguishable from Ac-6-FP treatment only, suggesting that eosinophilic activity *in situ* is modulated by resident MAIT cells.

To verify the ability of MAIT cells to activate eosinophils, and begin to translate our findings to humans, we incubated human whole blood with chemically synthesized MAIT cell agonist precursor 5-amino-6-D-ribitylaminouracil (5-A-RU) for 18 hours and assessed eosinophil activation through the upregulation of CD69 and human-leukocyte-associated antigen-DR (HLA-DR). Incubation of whole blood with 5-A-RU induced robust MAIT cell and eosinophil activation, which were both inhibited by MR1-specific blocking antibodies or Ac-6-FP (Fig. S7, A and B). 5-A-RU displayed similar eosinophil activation qualities to GM-CSF, the chosen positive control, with occasional discrepancies in HLA-DR upregulation (Fig. S7B). Expectedly, GM-CSF-induced eosinophil activation was MR1-independent and could not be blocked with Ac-6-FP.

**MR1, IL-4 and itch**

The pathogenesis and chronicity of AD can be mechanistically traced back to both innate and adaptive effector mechanisms, ultimately resulting in a heterogenous clinical presentation [20]. We therefore examined whether MAIT cells control other clinically relevant aspects of AD pathophysiology, in particular the production of the canonical Th2 cytokine IL-4 and chronic itch, two heavily pursued targets in the treatment of AD [39-41]. Our data revealed that the absence or therapeutic antagonism of MAIT cells is associated with significantly decreased levels of IL-4 protein *in situ* (Fig. 4A). This was confirmed transcriptionally in Ac-6-FP treated mice (Fig. 4B). Furthermore, the absence or therapeutic antagonism of MAIT cells also reduced MC903-induced itch (Fig. 4, C and D). The detection of IL-4 or IL-13 by sensory neurons has recently been shown to mediate chronic itch, and the development of skin pathology in an MC903-driven model of AD [42]. Previous work in our model showed basophils as the main producers of IL-4 [24], and basophil Il-4 secretion has also been revealed to control type 2 innate lymphoid cells (ILC2) expansion and IL-13 expression, to enhance skin inflammation in AD [43]. We therefore sought to determine the optimal time-point to study the potential interaction between MAIT cells and basophils and compared basophil frequency and function at days 9, 14 and 19 (Fig. 4E). For an unequivocal identification of basophils and the

quantification of basophil-derived IL-4 and IL-13 we used Basoph8 (B8)x4C13R mice [44,45]. A peak of basophil infiltration was observed at day 14 (Fig. 4F), which coincided with the time of maximal basophil-associated IL-4-production (Fig. 4G). Accordingly, in subsequent experiments, we shortened our MC903-driven model of AD to 15 days to investigate the mechanistic overlap between inducible basophil depletion and topical Ac-6-FP application.

**MR1-dependence of the cutaneous recruitment of basophils and other pruritogenic type 2 effector cells**

We used B8xiDTR mice to specifically deplete basophils [46]. Diphteria toxin (DT) was administered intraperitoneally, daily from day 9 to day 14, either by itself or combined with cutaneous application of Ac-6-FP (Fig. 5A). The depletion of basophils had a significantly impact on disease progression, as reflected by ear thickness measurements, but displayed a reduced therapeutic potency as compared to topical Ac-6-FP and did not provide any therapeutic benefit when combined with Ac-6-FP (Fig. 5, B and C). The depletion of basophils *in situ*, upon DT administration, was confirmed by flow cytometric quantification of YFP-expressing cells in tissue homogenates, which also revealed a significant, albeit not complete, reduction in skin-infiltrating basophils upon Ac-6-FP treatment (Fig. 5, D and E), suggesting that the cutaneous recruitment of basophils is partly MR1-dependent. Interestingly, the itch behaviors of basophil-depleted and Ac-6-FP only treated mice were identical, with no detectable therapeutic synergy (Fig. 5F), indicating that Ac-6-FP treatment targets basophils as well as other pruritogenic effector cells or mechanisms.

We confirmed that basophils are the predominant cell type producing IL-4 in this model of AD, with little co-expression of IL-13 (Fig. 5, G and H). However, Ac-6-FP, while strongly reducing the cutaneous recruitment of basophils, did not influence their ability to generate IL-4 (Fig. 5I), further supporting the notion that the anti-pruritic activity of Ac-6-FP is not solely operating via basophils, nor is IL-4 the only pruritogen. Since IL-4Rα, a significant driver of itch in AD patients [41], binds to IL-4 and IL-13, we next determined the identity of IL-13 producing cells and the capacity of Ac-6-FP to influence their cutaneous recruitment. Using B8xiDTRx4C13R mice, we observed that the main producers of IL-13 are $CD3^{high}$ dendritic epithelial T cells (DETC) [47], which accounted for half of IL-$13^+$ cells, followed by $CD3^+$ T cells and $CD3^-$ ILC (Fig. S8). Basophil-depletion reduced the

expression of IL-13 by both subsets, while Ac-6-FP treatment mainly influenced their recruitment (Fig. S8). These findings indicate that MAIT cells regulate the recruitment or expansion of all major type 2 cytokine secreting cell types.

**The immunosuppressive Effects of Narrowband UV-B Phototherapy are MR1- and folate-dependent**

Finally, we assessed the relevance of these combined findings for phototherapy, a well-established therapeutic option for cutaneous disease, including AD [20]. 6-FP is a photo-derivative of folic acid (the fully oxidized form of folate), which readily forms under UV-A or -B light in *in vitro* culture [48,49]. It is also a known oxidative degradation product of tetrahydrofolic acid (THF), which derives from ingested folic acid through the action of dihydrofolate reductase in the intestinal mucosa [50]. Studies in psoriasis patients have shown that folate blood levels are lowered by phototherapy, likely reflecting photolytic scission *in vivo* [21]. In the absence of any consensus regarding the mechanism of action of phototherapy [51], it is intriguing to consider that it may be at least partly mediated by MAIT cell antagonism. To address this, we determined, according to clinical practice, the narrowband UV-B (nbUVB) minimal erythema dose (MED) of our C57Bl/6 mouse colony. The established MED (500mJ/cm$^2$) could be safely administered without skin-related adverse reactions and reduced AD pathology in MC903-treated C57BL/6 mice but did not have any measurable impact on MR1-/- mice (Fig. 6, A and B). Similar observations were made for itch (Fig. 6C).

Next, we reasoned that the significant efficacy gap between phototherapy and the genetic deletion of MR1 may be due to the limited amount of folate available for photoconversion into 6-FP *in situ*. Indeed, both in humans and mice, folate is predominantly found in its reduced methylated form, 5-methyltetrahydrofolic acid (5MTHF) [52,53], which is similarly photo-labile but unable to release 6-FP upon photolysis [54]. We thus hypothesized that the therapeutic efficacy of phototherapy can be enhanced with prior topical application of folate. To test this hypothesis, we topically applied both photo-labile folate vitamers (separately, in their respective reduced form), 6S-THF (which releases 6-FP upon photolysis [50]) and 5MTHF, then compared their effects on subsequent phototherapy. Topical application of THF did indeed significantly increase the therapeutic efficacy of subsequent

phototherapy (MED, 500mJ/cm$^2$), leading to similar reductions in ear thickness (Fig. 6, D and E), TEWL (Fig. 6F) and epidermal (Fig. 6G) and dermal thickening (Fig. 6H) as observed with equimolar amounts of 6-FP. Notably, folate had intrinsic therapeutic activity against AD, which we attributed to the formation of 6-FP *via* oxidative degradation of folic acid [48], instead of photolysis. In contrast, no therapeutic enhancement of phototherapy was observed with topical application of 5MTHF (Fig. 6, E-H), which also did not display any therapeutic activity on its own.

**Discussion**

Atopic dermatitis (AD) is a multifaceted disease of complex etiology and heterogenous clinical presentation. The microbial colonization of the skin plays an influential role in the pathogenesis of AD [20], but the mechanism(s) linking the translocation of bacterial antigens across the characteristically abnormal skin barrier with chronic type 2 immune activation remain ill defined. Here, we identified MAIT cells as cutaneous immune sentinels which link bacterial sensing and type 2 effector functions. We found that MR1-dependent immune activation is required for the activation of skin-infiltrating eosinophils and the local recruitment of IL-4- and IL-13-producing cells. Importantly, this atopic checkpoint can be blocked with classically non-agonistic MR1 ligands, such as Ac-6-FP and 6-FP, which have therapeutic activity when applied topically or, in the case of 6-FP, generated *in vivo* via narrowband UVB phototherapy. While the binding of Ac-6-FP or 6-FP to MR1 can potentially activate smaller subsets of MR1-restricted T cells [55], the therapeutic activity observed with as yet exclusively non-agonistic compounds (Fig. S5) suggests that the treatment of atopic dermatitis is achieved through the inhibition of conventional MAIT cells.

The role MAIT cells play in disease is, in general, poorly understood. In humans, in the absence of biopsy material, the common observation is their disappearance from blood, generally assumed to reflect either their homing to tissue or decreased cell survival [56]. In the particular context of dermatological diseases, their frequency and function has been documented in human psoriasis and dermatitis herpetiformis patients, but their role in causing these diseases remains unclear [17,57]. In healthy human skin, MAIT cells are particularly enriched in the epidermis, consistent with an immune surveillance function. In mice, MAIT cells seem to preferentially reside in the dermis [58], although such comparison is confounded by the fact that the murine epidermis is seeded with γδ-TCR expressing dendritic epidermal T cells (DETC) during fetal development, thereby reducing the niche available for MAIT cells.

MAIT cells, like other innate-like T cells such as invariant Natural Killer T (iNKT) cells, have the capacity to mount potent responses to soluble signals, IL-12 and IL-18 in particular, and our results

suggest that skin-resident MAIT cells also belong to the restricted group of TSLP-responsive cell types [27] (Fig. 1I). Whether any particular combination of TCR/MR1-dependent and -independent activatory signals is required to induce pathogenic MAIT cell activation and overt disease remains to be investigated. However, it is intriguing to consider that the strong association between AD clinical outcome and *Staphylococcus aureus* colonization –and more specifically the associated production of superantigen (*e.g.* Staphylococcal Superantigen B; SEB) [59]– may reflect the potent effect of such combination [60].

Eosinophils and basophils are terminal type 2 effector cell types which are integral to atopic disease pathology [27]. As the topical application of Ac-6-FP was redundant with the conditional deletion of both of these effectors, the pathogenicity of cutaneous MAIT cell activation seems to depend on the downstream entrainment of their atopic effector functions. Importantly, the inhibition of MAIT cell activation only blocks eosinophilic activation, not their recruitment into inflamed skin. We therefore attribute the increased levels of wound healing observed in Ac-6-FP-treated mice (Fig. 2) to the additional tissue repair activity provided by incoming (homeostatic) eosinophils [61]. Due to the comparably low frequency of skin-resident MAIT cells, a contact-independent and/or indirect eosinophilic activation pathway seems likely and might extend to other organs as well, as both cell types reside in mucosae at steady-state. Of particular relevance, MAIT cells have been found to induce the rapid production of granulocyte-macrophage colony-stimulating factor (GM-CSF) in the lung [62].

In the MC903 model and others, basophils are an early innate source of IL-4 which drives the AD-specific epithelial immune microenvironment [63,64]. Here, we show that IL-4 expressing basophils steadily infiltrate the skin in an MR1-dependent and MR1-targetable manner. The significant link between MR1-dependent immune surveillance of the skin and pruritogenic effector mechanisms suggests that AD chronicity is driven by a self-perpetuating cycle of bacterial translocation, MAIT cell activation and itch, which might be initially precipitated by genetic factors affecting skin barrier integrity [20].

Ultraviolet therapy (phototherapy) is a widely used second line treatment for AD. Interestingly, we found that its therapeutic activity is MR1-dependent and can be increased by prior topical application of THF. While we did not attempt to detect and quantify 6-FP *in vivo* by mass spectrometry, the generation of 6-FP by photolysis of folate, its MR1-binding capacity and antagonistic activity on MAIT cell activation are well established. The ability of topical folate to enhance the therapeutic efficacy of phototherapy suggests that the subcutaneous availability of photocleavable folate is limiting. This is consistent with the strong compositional bias of circulating folate-derivates towards the 5-methyltetrahydrofolate form [53], which do not release 6-FP upon photolysis and do not synergize with phototherapy.

Collectively, this work demonstrates that MAIT cells are critical cutaneous immune sentinels, which rapidly respond to microbial challenge, and whose activation represents an important checkpoint for the release of atopic effector mechanisms. In this context we propose that, akin to vitamin D synthesis, photolysis of folic acid may represent a fundamental health benefit of solar radiation.

## Material and Methods

### Mice

Specific pathogen-free C57BL/6, MR1-/- [10] , Basoph8xiDTR, Basoph8x4C13RxiDTR [46], iPHIL (inducible eosinophil-deficient knock-in) [38] mice were used between 6-8 weeks of age and sex-matched for each experiment. Mice were housed at the Malaghan Institute of Medical Research Biomedical Research Unit and all experimental procedures were approved by the Victoria University Animal Ethics Committee and performed according to the institutional guidelines.

### Skin treatments

Mice were anaesthetized using i.p. ketamine/xylazine. MC903 (calcipotriol; Cayman Chemicals) was dissolved in 100% ethanol (EtOH) and topically applied on mouse ears (1nmol in 20μL per ear). As vehicle control, the same volume of EtOH was applied to the control group. Mice were treated 3 times a week for 19 days [24].

Acetyl-6-formylpterin (Ac-6-FP) and 6-formypterin (6-FP; both from Cayman chemicals) were both dissolved in 100% EtOH at a concentration of 1mg/mL (5mM) and topically applied daily from day 0 (prophylactically) or day 9 (therapeutically), until day 18. Luteolin, genistein and 3-formylsalicylic acid (3-FSA; all from Sigma) were similarly dissolved in 100% EtOH and applied daily from day 9.

An antibiotic cocktail comprised of polymyxin B, bacitracin and neomycin [29] (Sigma-Aldrich; 5000U/mL, 400U/mL and 3.5mg/mL, respectively, all in distilled water; 20μL applied per ear) was applied topically and daily from day -5 until day 16.

### Phototherapy and pretreatment with topical folate derivatives

5-methyltetrahydrofolic acid (5MTHF) and 6S-tetrahydrofolic acid (THF; both from Cayman chemicals) were dissolved in 70% EtOH at 5mM. 5MTHF and THF were topically applied to the skin (20μL per ear) on the days following MC903 treatment (as depicted in Fig. 6 D), with or without subsequent exposure to 500mJ/cm$^2$ narrowband ultraviolet B (UV-B) light. The DermaPal portable narrowband UV-B lamp (Daavlin) was used as the source of UV-B light for phototherapy. It emits UV-B light at wavelengths of 311-312nm and runs at 6.1mW/cm$^2$.

**Ear thickness measurements**

Ear thickness was measured while mice were sedated, using the TESA® Micromaster® digital caliper. Measurements were taken prior to each topical application of MC903 and at endpoint.

**Transepidermal water loss (TEWL) measurements**

TEWL was measured while mice were sedated, using the DERMALAB™ TEWL probe (Cortex Technology) at endpoint. TEWL was measured on both ears of the mice, at room temperature, and results were recorded once TEWL readings stabilized. Two readings from each ear were taken and averaged for each mouse.

**Histological evaluation and quantification**

Ear tissue was fixed in 4% PFA (Life Technologies) for 24 hours, processed, paraffin embedded and sectioned at 4μm. Slides were stained with haematoxylin & Eosin (H&E) and analyzed using a widefield microscope (Olympus BX51) with a 20X objective and the imaging software cellSens (Olympus GmbH). Measurements of the dermis and epidermis were quantified using Image J analysis [24].

**Confocal microscopy**

Ear tissue was incubated in 20% sucrose, snap frozen and subsequently cryosectioned at 8μm. Slides were fixed in 100% cold acetone for 3 minutes and then rinsed in PBS (Gibco). Next, slides were incubated with anti-mouse CD16/CD32 antibodies (generated from 24G2 hybridoma cells) to block non-specific antibody binding and incubated with the respective antibodies: purified anti-keratin 14 (Poly9060; Biolegend), secondary anti-chicken IgG antibody AF647 (Jackson Immuno Research), anti-Ki-67 eF450 (clone SolA15; eBioscience), anti-CD31 BV421 (clone 390; Biolegend), anti-vimentin AF488 (clone O91D3; Biolegend) and anti-SiglecF PE CF594 (clone E50-2440; BD). Slides were rinsed in PBS, mounted and visualized on a Laser Scanning Confocal Microscope FV1200 with an IX83 frame (Olympus). Images were obtained at both 40X and 20X objective. These images were subsequently assessed and quantified using Image J analysis.

**Tissue processing**

Single cell suspensions were prepared from ear tissue and spleen by mechanical disruption and passage through 70 μm nylon strainers (BD Falcon). For the skin harvest, ears were split into dorsal and ventral layers and digested with collagenase IV (Sigma-Aldrich) and DNaseI (Roche Diagnostics) for 30 minutes at 37 °C under agitation.

**Antibodies and flow cytometry**

Cells were re-suspended in PBS containing 1% FBS, 2mM EDTA (Invitrogen) and 0.01% sodium azide (Sigma-Aldrich) and incubated with anti-mouse CD16/CD32 antibody (generated from 24G2 hybridoma cells) to block non-specific antibody binding. Cell surface staining was conducted for 30 minutes using the monoclonal antibodies described below. Tetramer staining for MAIT cells (MR1-5-OP-RU, BV421 or PE labelled) was performed at room temperature according to the National Institute of Health (NIH) Tetramer Core Facility Instructions. Antibody to B220 (RA3-6B2), anti-CD4 (GK1.5), anti-CD11b (M1/70), anti-CD11c (HL3), anti-CD25 (PC61), anti-CD45.2 (104), anti-CD62L (MEL-14), anti-CD69 (H1.2F3), anti-CD90.2 (53-2.1), anti-CD117 (2B8), anti-Ly6G (1A8), anti-NK1.1 (PK136), anti-siglecF (E50-2440) were from BD Biosciences; anti-CD3 (17A2), anti-CD8a (53-6.7), anti-CD34 (MEC14.7), anti-CD44 (IM7), anti-CD64 (X54-5/7.1), anti-CD103 (2E7), anti-CD206 (CO68C2) anti-CD200R3 (Ba13) anti-CD274 (B7-H1), anti-γδ-TCR (GL3), anti-F4/80 (BM8), anti-Ly6 A/E (D7), anti-Ly6C (HK1.4), anti-PD-1 (RMPI-30), anti-TCR-β (H57-597) and anti-TSLP-R (22H9) were from Biolegend; anti-CD101 (REA301) was from Miltenyi Biotec and anti-ST2 (RMST2-2) was from eBioscience. Dead cells were excluded using DAPI (Molecular Probes) or Zombie Red Viability Kit (Biolegend). Data was acquired using a 3 laser Aurora spectral flow cytometer (Cytek) and analysed using FlowJo Software 10.5.3 (Treestar Inc.). Gating strategies are shown in Fig. S9.

**IL-4 quantification in tissue**

Ear samples were homogenized in PBS containing protease inhibitors (Halt™ protease inhibitor; Thermo Scientific) and 5 mM EDTA. Tissue lysates [44] were used to quantify IL-4 protein using an in-house ELISA kit. Tissue concentrations are expressed relative to total protein, as determined using a BCA™ protein assay kit (Thermo Scientific).

**Diptheria toxin (DT) treatment of iPHIL, B8xiDTR and B8xiDTRx4C13R mice**

DT (Sigma-Aldrich) was diluted in PBS and 20ng/g administered by i.p. injection every 3 days from day 6 for experiments using the iPHIL mice [24]. B8xiDTR mice were treated daily with 20ng/g of DT administered by i.p. for a maximum of 7 days.

**Itching frequency**

Mice behaviour was recorded for 30 minutes, at endpoint, and itch events determined and quantified by time-lapse videography [65].

**Quantitative Real Time PCR**

Quantitative real time PCR (q-PCR) was performed with cDNA generated from mouse ear tissue. First, RNA was extracted from tissue using Trizol™ reagent (ThermoFisher). Next, RNA to cDNA conversion was carried out using the Applied Qiagen Biosciences High–Capacity RNA-to-cDNA™ kit. Q-PCR analyses were conducted using the PowerUp SYBR Green gene expression master mix (Applied Biosystems), KiCqStart™ SYBR® Green primers (Sigma) for *Mmp10* (Matrix Mellatopeptidase 10, Gene ID:17384), *Mmp25* (Matrix Mellatopeptidase 25, Gene ID: 240047), *Furin* (paired basic amino acid cleaving enzyme, Gene ID: 8550) and *Il-4* (Interleukin 4, Gene ID: 16189) and a QuantStudio 7 real-time PCR system (Applied Biosystems). Applied Biosystems software was used to determine the cycle threshold (CT) value for each primer. ΔCT values were calculated and samples normalized to GAPDH control and compared with the EtOH-treated tissue.

**Whole blood activation assay**

Whole blood was obtained from healthy volunteers, as approved by the Victoria University of Wellington Human Ethics Committee and performed according to the institutional guidelines. Blood samples were mixed 1:1 with red blood cell lysis buffer (Sigma-Aldrich) and incubated for 15 minutes at 37 °C. Cells were washed once with PBS, then resuspended in the original volume in complete media (RPMI 1640, 10% FBS, 2mM L-glutamine, 55μM β-mercaptoethanol, 1% non-essential amino acids, 1mM sodium pyruvate, 100IU/ml Penicillin, 100μg/ml Streptomycin (Invitrogen). 200μL of the cell suspension were plated in wells of a 96 well U-bottom plate and incubated with 5-A-RU (45μM) or GM-CSF (Sigma; 50ng/mL), with or without Ac-6-FP (10μg/mL). Cells were incubated for 18 hours at 37°C before being processed and stained for flow cytometry. Samples were incubated with antibodies for 15 minutes at 4 °C, then washed and resuspended in FACS buffer (PBS, 1% FBS, 2mM EDTA (Invitrogen)). MAIT cells and eosinophils were identified as live $CD45^+CD3^+$TCR-V$\alpha$7.2$^+CD161^+$ and live $CD45^+$Siglec-$8^+$ cells, respectively.

Antibodies against CD45 (2D1), CD3 (UCHT1), TCR-Vα7.2 (3C10), CD161 (HP-3G10), Siglec-8 (7C9), CD69 (FN50), HLA-DR (L243) were all from Biolegend. Dead cells were excluded using DAPI (Molecular Probes) or Zombie Red Viability Kit (Biolegend). Data was acquired using a 3 laser Aurora spectral flow cytometer (Cytek) and analysed using FlowJo Software 10.5.3 (Treestar Inc.). Gating strategies are shown in Fig. S9.

**Chemical synthesis of MR1 ligands**

5-Amino-6-(D-ribitylamino)uracil (5-A-RU) was synthesized as previously described [66]. 5-Amino-6-(2-deoxy-D-ribitylamino)uracil (5-A-(2-deoxy)RU) [30,67] was prepared by reduction with 4.5 eq of sodium dithionite of the 5-nitroso-6-(2-deoxy-D-ribitylamino)uracil precursor [67], as previously described for 5-A-RU [66] and was stored at -80 ˚C until required for biological studies. Analysis by liquid chromatography–mass spectrometry (LC-MS) indicated the formation of 5-A-(2-deoxy)RU (Fig. S10). HRMS-ESI: m/z calcd for $C_9H_{17}N_4O_5$ $[M+H]^+$ 261.1199, found 261.1208. A comparable procedure using $D_2O$ was used to produce 5-A-(2-deoxy)RU for NMR analysis (Fig. S11): sodium dithionite (nominally 86% by redox titration, 52.0 mg, nominally 3.5 equiv) was added

to a suspension of the 5-nitroso-6-(2-deoxy-D-ribitylamino)uracil precursor (20 mg, 0.073 mmol) in deoxygenated $D_2O$ (1 mL). The mixture was briefly sonicated until the nitrosouracil dissolved and a colourless solution was obtained. $^1$H NMR (500 MHz, $D_2O$) δ 1.63-1.81 (m, 1H), 1.88-2.03 (m, 1H), 3.40-3.55 (m, 2H), 3.55-3.67 (m, 2H), 3.67-3.84 (m, 2H); $^{13}$C NMR (126 MHz, $D_2O$) δ 31.6, 38.7, 62.5, 69.2, 74.6, 91.2, 150.1, 151.2, 161.6.

5-(2-Oxopropylideneamino)-6-(2-deoxy-D-ribitylamino)uracil (5-OP-(2-deoxy)RU) was synthesized by a slightly modified literature procedure [68,69] . A solution of 5-A-(2-deoxy)RU (40 mg/mL) was adjusted to pH 7.0 with 1 M NaOH and lyophilized. The white solid was triturated with argon-sparged MeOH, filtered through an HPLC syringe filter to remove salts, and carefully concentrated under high vacuum. The solid was resuspended in argon-sparged sterile DMSO (10 mg/mL), and methylglyoxal (40% in water, 2 equiv) was added. The reaction stood for 45 minutes at room temperature and then was stored at -80 °C until required. Analysis by LC-MS (Fig. S10) indicated the formation of 5-OP-(2-deoxy)RU (m/z = 315.13 $[M + H]^+$; $R_t$ = 6.05 minutes, 95.5%, UV 265-360 nm), together with residual 5-A-(2-deoxy)RU (m/z = 261.12 $[M + H]^+$; $R_t$ = 1.69 minutes, 2.0%) and 7-methyl-8-(2-deoxy-D-ribityl) lumazine (m/z = 297.12 $[M + H]^+$; $R_t$ = 2.94 min, 2.5%). HRMS-ESI: m/z calculated for $C_{12}H_{19}N_4O_6$ = 5-OP-(2-deoxy)RU $[M + H]^+$ 315.1305, found 315.1316.

**Data visualization and statistics**

All graphical representation and statistical analyses of data was generated using Prism 7.0 or 8.0 (GraphPad Software). Statistics were calculated using one-way ANOVA with Tukey post-test or as indicated in the figure legend. Each data point represents an individual mouse ear or human participant. Plots show mean ± SEM. For the sake of optimal visualization, only relevant statistical results are shown.

**Author contributions:** KN, KW, CP, AC, DOS, KG, AJM, RJA, YL, AS, KP, JUM, AG, IFH, GP and EAJ contributed to investigation, methodology, data analysis and/or provided/synthesized key reagents. OG provided conceptualization, project administration and wrote the manuscript. All authors participated in discussion and interpretation of the results and commented on the manuscript.

**Competing interests:** The Malaghan Institute of Medical Research has filed a patent (pending) on the use of MR1 ligands in the context of inflammatory skin disease. The research presented herein was nevertheless carried out without any competing financial interests. No other disclosures were reported.

**Figure legends**

**Fig. 1. MR1-dependence of atopic dermatitis.** C57Bl/6 and MR1-/- mice were topically administered 1nmol MC903 or EtOH (vehicle control) for 19 days. (**A)** Ear thickness at each treatment timepoint and at endpoint. (**B)** Trans-epidermal water loss (TEWL) at endpoint. (**C-E)** Ear tissue sections stained with haematoxylin & eosin (H&E) at day 19 (scale bar = 100μm). (**C)** Representative H&E stained sections. Epidermal **(D)** and dermal **(E)** thickening quantified by Image J. **(F)** Representative dot plots for MAIT cell identification in ear and spleen. (**G)** MAIT cell frequency in untreated and MC903-treated ears. (**H)** CD4/CD8 co-receptor expression on MAIT cells isolated from the ears (pooled from 14 mice) and spleen of untreated and MC903-treated animals. (**I)** Phenotype of MAIT cells isolated from pooled ears of untreated and MC903-treated animals. Each data point represents an individual ear. Plots show mean ± SEM. Data represent three independent experiments. Statistics were calculated using one-way ANOVA with Tukey post-test., $^{**}P < 0.01$, $^{****}P < 0.001$, NS = non-significant.

**Fig. 2. MAIT cell inhibition reduces atopic dermatitis pathology and promotes wound healing.** C57Bl/6 and MR1-/- mice were topically administered 1nmol MC903 or EtOH (vehicle control) for 19 days. Ac-6-FP was topically applied from day 9 until day 18. (**A)** Schema of treatment regimen. **(B** and **C)** Ear thickness at each treatment timepoint (**B**) and endpoint (**C**). (**D)** TEWL at endpoint. (**E)** Expression of *Furin*, *Mmp10* and *Mmp25*, as assessed by q-PCR. (**F)** Representative confocal imaging of ear tissue sections stained for CD31 (blue), vimentin (green), keratin 14 (red) and SiglecF (magenta); volume projected along the z axis. (**G)** Area of CD31 and vimentin, and percentage of Ki-$67^{+}K14^{+}$ cells in each high-power field (HPF). Each data point represents an individual ear. Plots show mean ± SEM. Data represent three independent experiments. Statistics were calculated using one-way ANOVA with Tukey post-test. $^{**}P < 0.01$, *** $0.01 < P < 0.001$, $^{****}P < 0.001$, NS = non-significant.

**Fig. 3. MAIT cells control eosinophil activation in atopic dermatitis. (A-D)** C57Bl/6, iPHIL and MR1-/- mice were topically administered 1nmol MC903 or EtOH (vehicle control) for 19 days. Ac-6-FP was applied daily from day 9 until day 18. Assessment of eosinophil **(A)** frequency and **(B)** activation in skin tissue by flow cytometry. (**C** and **D)** Ear tissue was stained with anti-SiglecF antibodies (magenta) to detect and quantify eosinophils in the skin. (**C)** Representative confocal imaging of skin-infiltrating eosinophils; scale bar = 50μm. (**D)** Eosinophil number per high-power field (HPF). (**E-I)** iPHIL mice received diptheria toxin intraperitoneally alongside topical treatment of Ac-6-FP as described above. (**E)** Schema of treatment regimen. (**F)** Ear thickness at each treatment timepoint and **(G)** endpoint. (**H)** TEWL at endpoint. (**I)** Epidermal and dermal thickening. Each data point represents an individual ear. Plots show mean ± SEM. Data represent three independent experiments. Statistics were calculated using one-way ANOVA with Tukey post-test. **P* <0.05, ***P* <0.01, *** 0.01< *P* <0.001, *****P* <0.001, NS = non-significant.

**Fig. 4. MAIT cell inhibition reduces IL-4 production and itch. (A-D)** C57Bl/6 or MR1-/- mice were topically administered 1nmol MC903 or EtOH (vehicle control) for 19 days. Ac-6-FP was applied daily from day 9 until day 18. IL-4 levels were evaluated at endpoint in ear tissue by **(A)** ELISA and **(B)** q-PCR. Itching/scratching events were quantified by time-lapse videography and expressed as itching events per mouse within a 30-minute timeframe in **(C)** MR1-/- mice and **(D)** Ac-6-FP-treated wild-type mice. (**E-G)** Basoph8x4C13R mice were topically administered 1nmol MC903 or EtOH (vehicle control) for either 9, 14 or 19 days (treatment regimen shown in **(E)**). (**F)** The frequency of basophils *in situ* and **(G)** the respective percentage of IL-4-producing basophils were determined for each endpoint. Each data point represents an individual ear or mouse. Plots show mean ± SEM. Data represent three independent experiments. Statistics were calculated using one-way ANOVA with Tukey post-test. **P* <0.05, ***P* <0.01, *** 0.01< *P* <0.001, *****P* <0.001.

**Fig. 5. MAIT cell inhibition blocks basophil-mediated pathology.** C57Bl/6, basoph8(B8)xiDTR or B8xiDTRx4C13R mice were topically administered 1nmol MC903 or EtOH (vehicle control) for 14 days (endpoint for all experiments was day 15). **(A)** Schema of treatment regimen. (**B** and **C)** Ear thickness at **(B)** each treatment timepoint and **(C)** endpoint. (**D)** Basophils were identified by YFP-

expression in B8 mice and **(E)** their frequencies were determined at endpoint in Ac-6-FP-treated mice in the presence or absence of DT treatment. (**F)** Itching/scratching events as quantified by time-lapse videography. (**G-I)** Cytokine production by ($YFP^+$) basophils and non-basophils ($YFP^-$) was quantified by AmCyan (IL-4) and DsRed (IL-13) reporter expression. (**G)** Representative dot plots depicting IL-4 production from $YFP^+$ (basophils) and $YFP^-$ cells at day 15. (**H)** IL-4/IL-13 co-expression from basophils following various treatments. (**I)** Impact of Ac-6-FP treatment on IL-4 secretion by basophils. Each data point represents an individual ear or mouse. Plots show mean ± SEM. Data represent three independent experiments. Statistics were calculated using one-way ANOVA with Tukey post-test. $^{**}P < 0.01$, *** $0.01 < P < 0.001$, $^{****}P < 0.001$, NS = non-significant.

**Fig. 6. Application of folate derivatives enhances the therapeutic efficacy of phototherapy against atopic dermatitis**. **(A-C)** C57Bl/6 or MR1-/- mice were topically administered MC903 for 18 days. Ears were exposed to 500mJ/cm$^2$ UV-B on the day following MC903 application with the last UV-B exposure on day 17. (**A)** Ear thickness, **(B)** TEWL and **(C)** itch behavior at endpoint. **(D-H)** C57Bl/6 mice were topically administered 1nmol MC903 or EtOH (vehicle control) for 19 days. Ears were treated with either 6S-tetrahydrofolate (THF, which releases 6-FP upon photolysis) or 5-methyltetrahydrofolate (5MTHF, which does not release 6-FP upon photolysis) on the days following MC903 application and prior to phototherapy (500mJ/cm$^2$ UV-B exposure). (**D)** Schema of treatment regimen. (**E-H)** Endpoint measurements of **(E)** ear thickness, **(F)** TEWL, **(G)** epidermal and **(H)** dermal thickening. Each data point represents an individual ear. Plots show mean ± SEM. Data represent three independent experiments. Statistics were calculated using one-way ANOVA with Tukey post-test. $^{*}P < 0.05$, $^{**}P < 0.01$, $^{****}P < 0.001$, NS = non-significant.

**Fig. S1. Bacterial colonization of the skin is necessary to induce atopic dermatitis.** C57Bl/6 and MR1-/- mice were topically administered 1nmol MC903 or EtOH (vehicle control) for 19 days. An antibiotic cocktail of polymyxin B, bacitracin and neomycin (5000U/mL, 400U/mL and 3.5mg/mL, respectively) was topically applied daily from day -5. (**A)** Schema of treatment regimen. (**B)** Ear thickness at endpoint. (**C)** TEWL at endpoint. (**D)** ELISA quantification of TSLP serum levels at day 9. ND = not detected. Plots show mean ± SEM. Each data point represents an individual ear. Data

represent 3 independent experiments. Statistics were calculated using one-way ANOVA with Tukey post-test. *** $0.01 < P < 0.001$, **** $P < 0.001$, NS = non-significant.

**Fig. S2. Prophylactic inhibition of MAIT cell activation reduces atopic dermatitis pathology.** C57Bl/6 mice were topically administered 1nmol MC903 or EtOH (vehicle control) for 19 days. 6-FP or Ac-6-FP was applied daily from day 0 until day 18. (**A)** Schema of treatment regimen. (**B** and **C)** Ear thickness at **(B)** each treatment timepoint and **(C)** endpoint. (**D)** TEWL at endpoint. (**E** and **F)** Tissue sections were stained with H&E and **(E)** epidermal and **(F)** dermal thickening quantified by Image J analysis. Plots show mean ± SEM. Each data point represents an individual ear. Data represent three independent experiments. Statistics were calculated using one-way ANOVA with Tukey post-test. * $P < 0.05$, ** $P < 0.01$, *** $0.01 < P < 0.001$, **** $P < 0.001$, NS = non-significant.

**Fig. S3. Dose-dependent therapeutic efficacy of Ac-6-FP against atopic dermatitis.** C57Bl/6 mice were topically administered 1nmol MC903 or EtOH (vehicle control) for 19 days. Ac-6-FP, in doses ranging from 1.25mM to 5mM, was therapeutically applied from day 9 until day 18 and ear thickness determined at endpoint. Plots show mean ± SEM. Each data point represents an individual ear. Statistics were calculated using one-way ANOVA with Tukey post-test. ** $P < 0.01$, **** $P < 0.001$.

**Fig. S4. Therapeutic efficacy of 6-FP against atopic dermatitis.** C57Bl/6 mice were topically administered 1nmol MC903 or EtOH (vehicle control) for 19 days. 6-FP was applied daily from day 9 until day 18. (**A)** Schema of treatment regimen. (**B** and **C)** Ear thickness was measured at **(B)** each treatment timepoint and **(C)** endpoint. (**D)** TEWL at endpoint. Plots show mean ± SEM. Each data point represents an individual ear. Data represent three independent experiments. Statistics were calculated using one-way ANOVA with Tukey post-test. ** $P < 0.01$, **** $P < 0.001$, NS = non-significant.

**Fig. S5. Therapeutic activity of structurally distinct MAIT cell antagonists.** C57Bl/6 mice were topically administered 1nmol MC903 or EtOH (vehicle control) for 19 days. MAIT cell antagonists were topically applied from day 9 until day 18. (**A)** Schema of treatment regimen. **(B** and **C)** Endpoint

ear thickness after treatment with Ac-6-FP, 3-formylsalicylic acid (3-FSA), luteolin and genistein (**B**) as well as 5-(2-oxopropylideneamino)-6-(2-deoxy)-D-ribitylaminouracil (5-OP-(2-deoxy)RU) and 5-amino-6-(2-deoxy)-D-ribitylaminouracil (5-A-(2-deoxy)RU) (**C**). (**D)** TEWL at endpoint following treatment with 5-OP-(2-deoxy)RU and 5-A-(2-deoxy)RU. Each data point represents an individual ear. Plots show mean ± SEM. Statistics were calculated using one-way ANOVA with Dunnett's post-test comparing ear thickness or TEWL observed with MC903-only with the values obtained after therapeutic treatment with the different MAIT cell antagonists. **P* <0.05, ***P* <0.01, *** 0.01< *P* <0.001, *****P* <0.001, NS = non-significant.

**Fig. S6. Genetic deletion of MR1 does not reduce eosinophil infiltration in atopic dermatitis. (A-B)** C57Bl/6 and MR1-/- mice were topically administered 1nmol MC903 or EtOH (vehicle control) for 19 days. Assessment of eosinophil **(A)** numbers and **(B)** frequency in skin tissue by flow cytometry at endpoint. Each data point represents an individual ear. Plots show mean ± SEM. Statistics were calculated using one-way ANOVA with Tukey post-test. ***P* <0.01, NS = non-significant.

**Fig. S7. MAIT cell activation with the microbial metabolite 5-A-RU leads to eosinophil activation in human blood.** Whole human blood was incubated for 18 hours with the MAIT cell-specific agonist 5-amino-6-D-ribitylaminouracil (5-A-RU) and MAIT cell as well as eosinophil activation assessed by flow cytometry. Frequency of activated **(A)** MAIT cells ($CD69^+$) and **(B)** eosinophils ($CD69^+$ or $HLA\text{-}DR^+$) following whole blood activation with 5-A-RU in the presence or absence of blocking anti-MR1 antibodies or Ac-6-FP. GM-CSF was used as a positive control for eosinophil activation, with different activation profiles observed in human blood donors (as shown for HD#2 and HD#3). Data represent three independent experiments. Each condition was run in duplicate. Plots show mean ± SEM. Statistics were calculated using one-way ANOVA with Dunnett's post-test comparing the level of cellular activation observed with 5-A-RU-only with the ones observed upon MR1 blockade. *** 0.01< *P* <0.001, *****P* <0.001.

**Fig. S8. MAIT cell inhibition reduces the number of IL-13-producing cells *in situ*.** C57Bl/6 or B8xiDTRx4C13R mice were topically administered 1nmol MC903 or EtOH (vehicle control) for 14 days (endpoint for all experiments was day 15). Ear tissue was harvested, digested and the number and phenotype of DETCs, ILC2s and $CD4^+$ T cells were determined by flow cytometry. **(A)** Representative dot plots of IL-13 reporter expression from $CD3^-$, $CD3^+$ and $CD3^{high}$ cells (broadly representing ILCs, Th2 and DETCs, respectively). (**B** and **C)** Total number and frequency of IL-$13^+$ DETCs. (**D** and **E)** Total number and frequency of IL-$13^+$ ILCs in the skin ($CD45^+CD64^-Ly6G^-SiglecF^-NK1.1^-CD90.2^+$). (**F** and **G)** total number and frequency of IL-$13^+$ $CD4^+$ T cells ($CD3^+CD4^+$). Each data point represents an individual ear or mouse. Plots show mean ± SEM. Statistics were calculated using one-way ANOVA with Tukey post-test. ** $P$ <0.01, *** 0.01< $P$ <0.001, **** $P$ <0.001, NS = non-significant.

**Fig. S9. Flow cytometry gating strategies.** (**A-C)** C57Bl/6 or B8xiDTRx4C13R mice were euthanised at endpoint and ear tissue was harvested and digested. Single cell suspensions were stained with the specific antibody cocktails or the MR1-5-OP-RU tetramer. (**A)** Representative dot plots for gating strategy of MAIT cells. (**B)** Representative dot plots for gating strategy of ILC2s in the skin. (**C)** Representative dot plot of YFP reporter expression in B8 mice to identify basophils. Pre-gating of live cells, CD45+ cells was conducted. (**D)** Gating strategy for MAIT cells and eosinophils in human whole blood.

**Fig. S10. LCMS chromatograms of 5-A-(2-deoxy)RU and 5-OP-(2-deoxy)RU.** Top panel; A freshly prepared solution of 5-A-(2-deoxy)RU (5 mg/mL, DMSO) was diluted into deoxygenated water (0.5 mg/mL) for LCMS analysis. Bottom panel; Crude reaction between 5-A-(2-deoxy)RU (10 mg/mL DMSO) and methylglyoxal (2 equiv). After a 30 mins incubation period, an aliquot was diluted into deoxygenated water (0.5 mg/mL) for analysis. LC-MS analysis was performed on a Waters Acquity UPLC H-Class system equipped with a Waters Xevo G2-XS Q-TOF tandem mass spectroscopic detector. A Phenomenex Synergi Fusion-RP column (2.5 μm, 100 A°, 50 × 3 mm) was used with A = 10 mM aqueous ammonium acetate (pH 5.2) and B = MeOH: 0-2 mins, 100% A; 2-7 mins, 0-50% B; 7-8 mins, 50-100% B; 8-10 mins, 100% B; 0.5 mL/min, 40 °C. The products were

identified using a scanning diode array detector (265-360 nm) and electrospray ionization in positive mode.

**Fig. S11. $^{1}H$ and $^{13}C$ NMR spectra of 5-amino-6-(2-deoxy-D-ribitylamino)uracil in $D_2O$.**

**References**


1. Le Bourhis L, Guerri L, Dusseaux M, Martin E, Soudais C, Lantz O. Mucosal-associated invariant T cells: unconventional development and function. *Trends Immunol.* 2011;32(5):212-218.

2. Mori L, Lepore M, De Libero G. The Immunology of CD1- and MR1-Restricted T Cells. *Annu Rev Immunol.* 2016;34:479-510.

3. Ussher JE, Klenerman P, Willberg CB. Mucosal-associated invariant T-cells: new players in anti-bacterial immunity. *Front Immunol.* 2014;5(450):450.

4. Dusseaux M, Martin E, Serriari N, et al. Human MAIT cells are xenobiotic-resistant, tissue-targeted, CD161hi IL-17-secreting T cells. *Blood.* 2011;117(4):1250-1259.

5. Le Bourhis L, Martin E, Peguillet I, et al. Antimicrobial activity of mucosal-associated invariant T cells. *Nat Immunol.* 2010;11(8):701-708.

6. Martin E, Treiner E, Duban L, et al. Stepwise development of MAIT cells in mouse and human. *PLoS Biol.* 2009;7(3):e54.

7. Tang XZ, Jo J, Tan AT, et al. IL-7 licenses activation of human liver intrasinusoidal mucosal-associated invariant T cells. *J Immunol.* 2013;190(7):3142-3152.

8. Keller AN, Corbett AJ, Wubben JM, McCluskey J, Rossjohn J. MAIT cells and MR1-antigen recognition. *Curr Opin Immunol.* 2017;46:66-74.

9. Kjer-Nielsen L, Patel O, Corbett AJ, et al. MR1 presents microbial vitamin B metabolites to MAIT cells. *Nature.* 2012;491(7426):717-723.

10. Treiner E, Duban L, Bahram S, et al. Selection of evolutionarily conserved mucosal-associated invariant T cells by MR1. *Nature.* 2003;422(6928):164-169.

11. Wang H, D'Souza C, Lim XY, et al. MAIT cells protect against pulmonary Legionella longbeachae infection. *Nat Commun.* 2018;9(1):3350.

12. Wilgenburg BV, Loh L, Chen Z, et al. MAIT cells contribute to protection against lethal influenza infection in vivo. *Nat Commun.* 2018;9(1):4706.

13. Huang S, Martin E, Kim S, et al. MR1 antigen presentation to mucosal-associated invariant T cells was highly conserved in evolution. *Proc Natl Acad Sci U S A.* 2009;106(20):8290-8295.

14. Leeansyah E, Loh L, Nixon DF, Sandberg JK. Acquisition of innate-like microbial reactivity in mucosal tissues during human fetal MAIT-cell development. *Nat Commun.* 2014;5(3143):3143.

15. Hegde P, Weiss E, Paradis V, et al. Mucosal-associated invariant T cells are a profibrogenic immune cell population in the liver. *Nat Commun.* 2018;9(1):2146.

16. Rouxel O, Da Silva J, Beaudoin L, et al. Cytotoxic and regulatory roles of mucosal-associated invariant T cells in type 1 diabetes. *Nat Immunol.* 2017;18(12):1321-1331.

17. Li J, Reantragoon R, Kostenko L, Corbett AJ, Varigos G, Carbone FR. The frequency of mucosal-associated invariant T cells is selectively increased in dermatitis herpetiformis. *Australas J Dermatol.* 2017;58(3):200-204.

18. Chen YE, Fischbach MA, Belkaid Y. Skin microbiota-host interactions. *Nature.* 2018;553(7689):427-436.

19. Linehan JL, Harrison OJ, Han SJ, et al. Non-classical Immunity Controls Microbiota Impact on Skin Immunity and Tissue Repair. *Cell.* 2018;172(4):784-796 e718.

20. Weidinger S, Beck LA, Bieber T, Kabashima K, Irvine AD. Atopic dermatitis. *Nat Rev Dis Primers.* 2018;4(1):1.

21. Juzeniene A, Stokke KT, Thune P, Moan J. Pilot study of folate status in healthy volunteers and in patients with psoriasis before and after UV exposure. *J Photochem Photobiol B.* 2010;101(2):111-116.

22. Valencia-Vera E, Aguilera J, Cobos A, Bernabo JL, Perez-Valero V, Herrera-Ceballos E. Association between seasonal serum folate levels and ultraviolet radiation. *J Photochem Photobiol B.* 2019;190:66-71.

23. Eckle SB, Birkinshaw RW, Kostenko L, et al. A molecular basis underpinning the T cell receptor heterogeneity of mucosal-associated invariant T cells. *J Exp Med.* 2014;211(8):1585-1600.

24. Naidoo K, Jagot F, van den Elsen L, et al. Eosinophils determine dermal thickening and water loss in a MC903 model of atopic dermatitis. *J Invest Dermatol.* 2018;28(18):32227-32229.

25. Holm EA, Wulf HC, Thomassen L, Jemec GB. Instrumental assessment of atopic eczema: validation of transepidermal water loss, stratum corneum hydration, erythema, scaling, and edema. *J Am Acad Dermatol.* 2006;55(5):772-780.

26. Zhou B, Comeau MR, De Smedt T, et al. Thymic stromal lymphopoietin as a key initiator of allergic airway inflammation in mice. *Nat Immunol.* 2005;6(10):1047-1053.

27. Ziegler SF, Artis D. Sensing the outside world: TSLP regulates barrier immunity. *Nat Immunol.* 2010;11(4):289-293.

28. Salou M, Legoux F, Gilet J, et al. A common transcriptomic program acquired in the thymus defines tissue residency of MAIT and NKT subsets. *J Exp Med.* 2018;5(20181483):20181483.

29. SanMiguel AJ, Meisel JS, Horwinski J, Zheng Q, Grice EA. Topical Antimicrobial Treatments Can Elicit Shifts to Resident Skin Bacterial Communities and Reduce Colonization by Staphylococcus aureus Competitors. *Antimicrob Agents Chemother.* 2017;61(9).

30. Braganza CD, Shibata K, Fujiwara A, et al. The effect of MR1 ligand glyco-analogues on mucosal-associated invariant T (MAIT) cell activation. *Org Biomol Chem.* 2019:DOI: 10.1039/C1039OB01436E.

31. Keller AN, Eckle SB, Xu W, et al. Drugs and drug-like molecules can modulate the function of mucosal-associated invariant T cells. *Nat Immunol.* 2017;18(4):402-411.

32. Werner S, Grose R. Regulation of wound healing by growth factors and cytokines. *Physiol Rev.* 2003;83(3):835-870.

33. Cheng F, Shen Y, Mohanasundaram P, et al. Vimentin coordinates fibroblast proliferation and keratinocyte differentiation in wound healing via TGF-beta-Slug signaling. *Proc Natl Acad Sci U S A.* 2016;113(30):E4320-4327.

34. Sauter B, Foedinger D, Sterniczky B, Wolff K, Rappersberger K. Immunoelectron microscopic characterization of human dermal lymphatic microvascular endothelial cells. Differential expression of CD31, CD34, and type IV collagen with lymphatic endothelial cells vs blood capillary endothelial cells in normal human skin, lymphangioma, and hemangioma in situ. *J Histochem Cytochem.* 1998;46(2):165-176.

35. Abdala-Valencia H, Coden ME, Chiarella SE, et al. Shaping eosinophil identity in the tissue contexts of development, homeostasis, and disease. *J Leukoc Biol.* 2018;104(1):95-108.

36. Bochner BS. Systemic activation of basophils and eosinophils: markers and consequences. *J Allergy Clin Immunol.* 2000;106(5 Suppl):S292-302.

37. Gonzalez-Amaro R, Cortes JR, Sanchez-Madrid F, Martin P. Is CD69 an effective brake to control inflammatory diseases? *Trends Mol Med.* 2013;19(10):625-632.

38. Jacobsen EA, Lesuer WE, Willetts L, et al. Eosinophil activities modulate the immune/inflammatory character of allergic respiratory responses in mice. *Allergy.* 2014;69(3):315-327.

39. Chang HY, Nadeau KC. IL-4Ralpha Inhibitor for Atopic Disease. *Cell.* 2017;170(2):222.

40. Ruzicka T, Hanifin JM, Furue M, et al. Anti-Interleukin-31 Receptor A Antibody for Atopic Dermatitis. *N Engl J Med.* 2017;376(9):826-835.

41. Simpson EL, Bieber T, Guttman-Yassky E, et al. Two Phase 3 Trials of Dupilumab versus Placebo in Atopic Dermatitis. *N Engl J Med.* 2016;375(24):2335-2348.

42. Oetjen LK, Mack MR, Feng J, et al. Sensory Neurons Co-opt Classical Immune Signaling Pathways to Mediate Chronic Itch. *Cell.* 2017;171(1):217-228 e213.

43. Kim BS, Wang K, Siracusa MC, et al. Basophils promote innate lymphoid cell responses in inflamed skin. *J Immunol.* 2014;193(7):3717-3725.

44. Roediger B, Kyle R, Yip KH, et al. Cutaneous immunosurveillance and regulation of inflammation by group 2 innate lymphoid cells. *Nat Immunol.* 2013;14(6):564-573.

45. Sullivan BM, Liang HE, Bando JK, et al. Genetic analysis of basophil function in vivo. *Nat Immunol.* 2011;12(6):527-535.

46. Pellefigues C, Mehta P, Prout MS, et al. The Basoph8 Mice Enable an Unbiased Detection and a Conditional Depletion of Basophils. *Front Immunol.* 2019;10:2143.

47. Tong PL, Roediger B, Kolesnikoff N, et al. The skin immune atlas: three-dimensional analysis of cutaneous leukocyte subsets by multiphoton microscopy. *J Invest Dermatol.* 2015;135(1):84-93.

48. Gazzali AM, Lobry M, Colombeau L, et al. Stability of folic acid under several parameters. *Eur J Pharm Sci.* 2016;93:419-430.

49. Juzeniene A, Grigalavicius M, Ma LW, Juraleviciute M. Folic acid and its photoproducts, 6-formylpterin and pterin-6-carboxylic acid, as generators of reactive oxygen species in skin cells during UVA exposure. *J Photochem Photobiol B.* 2016;155:116-121.

50. Reed LS, Archer MC. Oxidation of tetrahydrofolic acid by air. *J Agric Food Chem.* 1980;28(4):801-805.

51. Hart PH, Gorman S, Finlay-Jones JJ. Modulation of the immune system by UV radiation: more than just the effects of vitamin D? *Nat Rev Immunol.* 2011;11(9):584-596.

52. Kopp M, Morisset R, Koehler P, Rychlik M. Stable Isotope Dilution Assays for Clinical Analyses of Folates and Other One-Carbon Metabolites: Application to Folate-Deficiency Studies. *PLoS One.* 2016;11(6):e0156610.

53. Pfeiffer CM, Sternberg MR, Fazili Z, et al. Folate status and concentrations of serum folate forms in the US population: National Health and Nutrition Examination Survey 2011-2. *Br J Nutr.* 2015;113(12):1965-1977.

54. Steindal AH, Juzeniene A, Johnsson A, Moan J. Photodegradation of 5-methyltetrahydrofolate: biophysical aspects. *Photochem Photobiol.* 2006;82(6):1651-1655.

55. Gherardin NA, Keller AN, Woolley RE, et al. Diversity of T Cells Restricted by the MHC Class I-Related Molecule MR1 Facilitates Differential Antigen Recognition. *Immunity.* 2016;44(1):32-45.

56. Rouxel O, Lehuen A. Mucosal-associated invariant T cells in autoimmune and immune-mediated diseases. *Immunol Cell Biol.* 2018;96(6):618-629.

57. Teunissen MBM, Yeremenko NG, Baeten DLP, et al. The IL-17A-producing CD8+ T-cell population in psoriatic lesional skin comprises mucosa-associated invariant T cells and conventional T cells. *J Invest Dermatol.* 2014;134(12):2898-2907.

58. Constantinides MG, Link VM, Tamoutounour S, et al. MAIT cells are imprinted by the microbiota in early life and promote tissue repair. *Science.* 2019;366(6464).

59. Schlievert PM, Case LC, Strandberg KL, Abrams BB, Leung DY. Superantigen profile of Staphylococcus aureus isolates from patients with steroid-resistant atopic dermatitis. *Clin Infect Dis.* 2008;46(10):1562-1567.

60. Shaler CR, Choi J, Rudak PT, et al. MAIT cells launch a rapid, robust and distinct hyperinflammatory response to bacterial superantigens and quickly acquire an anergic phenotype that impedes their cognate antimicrobial function: Defining a novel mechanism of superantigen-induced immunopathology and immunosuppression. *PLoS Biol.* 2017;15(6):e2001930.

61. Weller PF, Spencer LA. Functions of tissue-resident eosinophils. *Nat Rev Immunol.* 2017;17(12):746-760.

62. Meierovics AI, Cowley SC. MAIT cells promote inflammatory monocyte differentiation into dendritic cells during pulmonary intracellular infection. *J Exp Med.* 2016;213(12):2793-2809.

63. Dainichi T, Kitoh A, Otsuka A, et al. The epithelial immune microenvironment (EIME) in atopic dermatitis and psoriasis. *Nat Immunol.* 2018;19(12):1286-1298.

64. Karasuyama H, Miyake K, Yoshikawa S, Yamanishi Y. Multifaceted roles of basophils in health and disease. *J Allergy Clin Immunol.* 2018;142(2):370-380.

65. Lee JJ, Protheroe CA, Luo H, et al. Eosinophil-dependent skin innervation and itching following contact toxicant exposure in mice. *The Journal of allergy and clinical immunology.* 2014.

66. Lange J, Anderson RJ, Marshall AJ, et al. The Chemical Synthesis, Stability, and Activity of MAIT Cell Prodrug Agonists That Access MR1 in Recycling Endosomes. *ACS Chem Biol.* 2020;15(2):437-445.

67. Ler GJM, Xu W, Mak JYW, Liu L, Bernhardt PV, Fairlie DP. Computer Modelling and Synthesis of Deoxy and Monohydroxy Analogues of a Ribitylaminouracil Bacterial Metabolite that Potently Activates Human T Cells. *Chemistry.* 2019;25(68):15594-15608.

68. Corbett AJ, Eckle SB, Birkinshaw RW, et al. T-cell activation by transitory neo-antigens derived from distinct microbial pathways. *Nature.* 2014;509(7500):361-365.

69. Mak JY, Xu W, Reid RC, et al. Stabilizing short-lived Schiff base derivatives of 5-aminouracils that activate mucosal-associated invariant T cells. *Nat Commun.* 2017;8:14599.

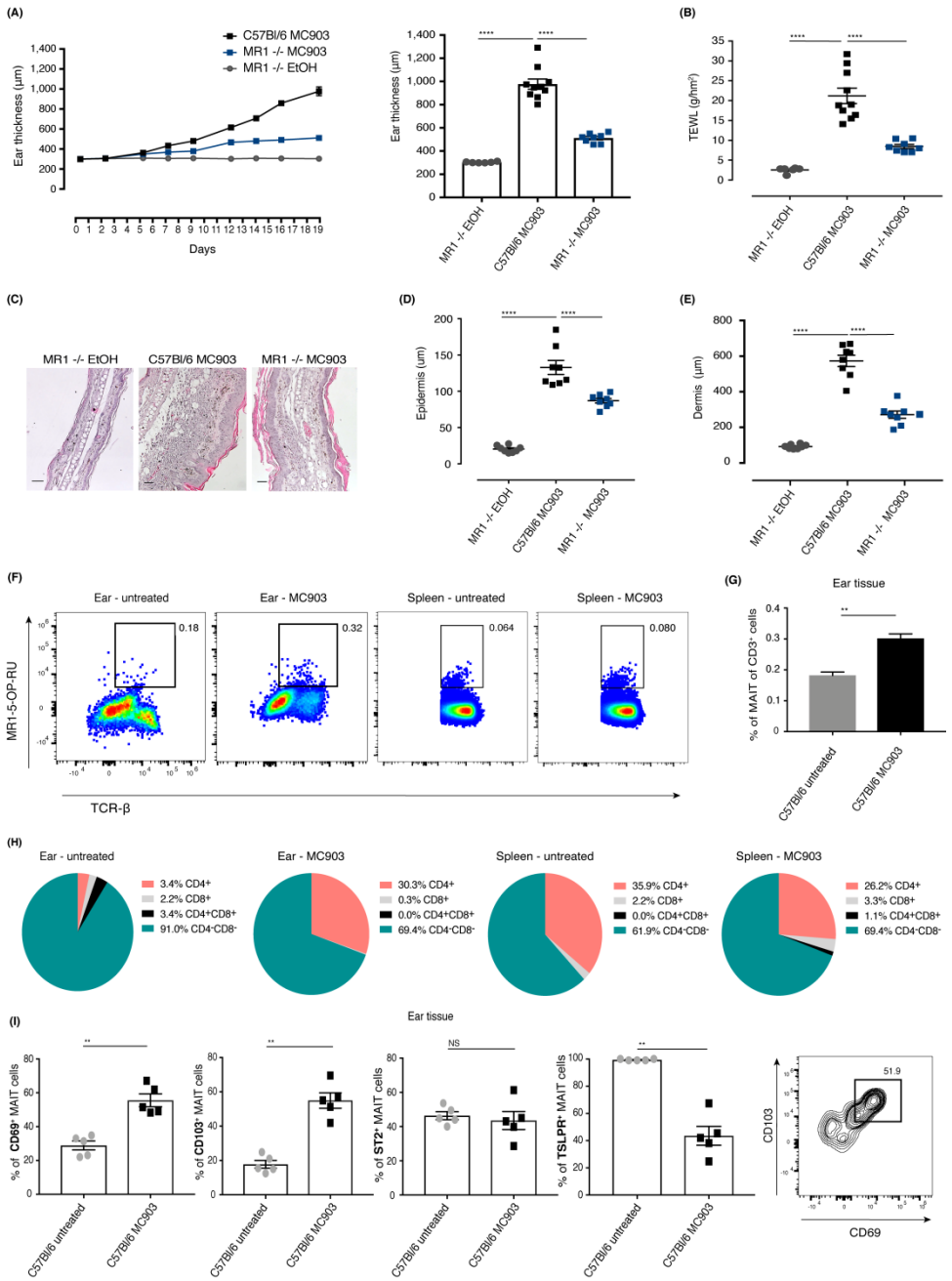


all_14994_f1.tif

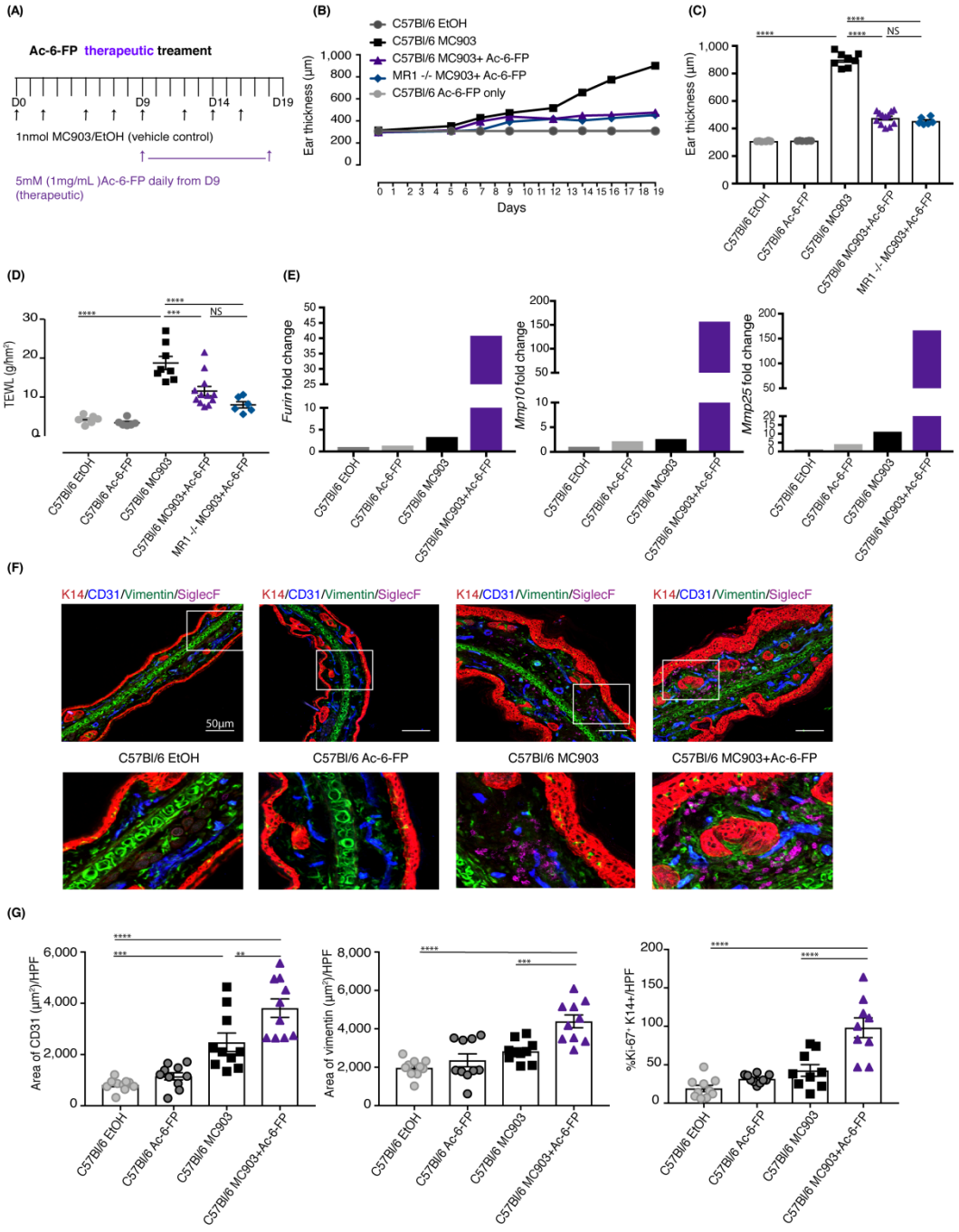


all_14994_f2.tif

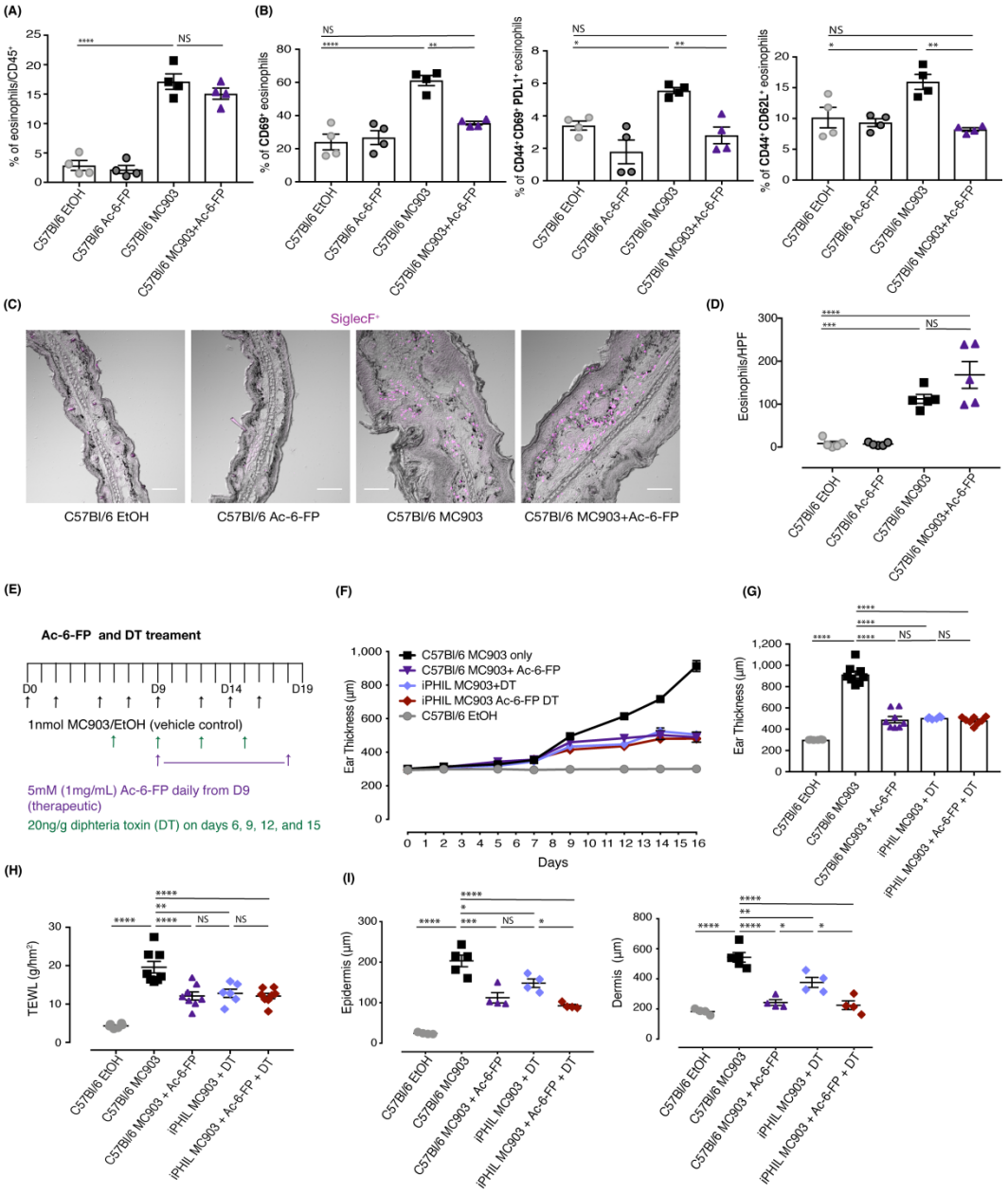


all_14994_f3.tif

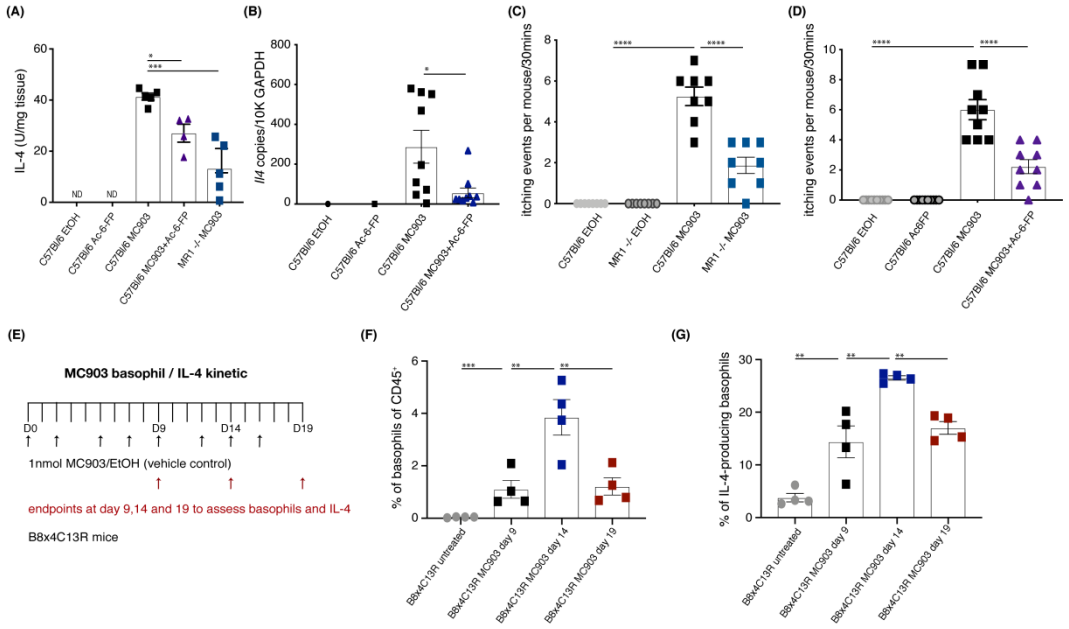


all_14994_f4.tif

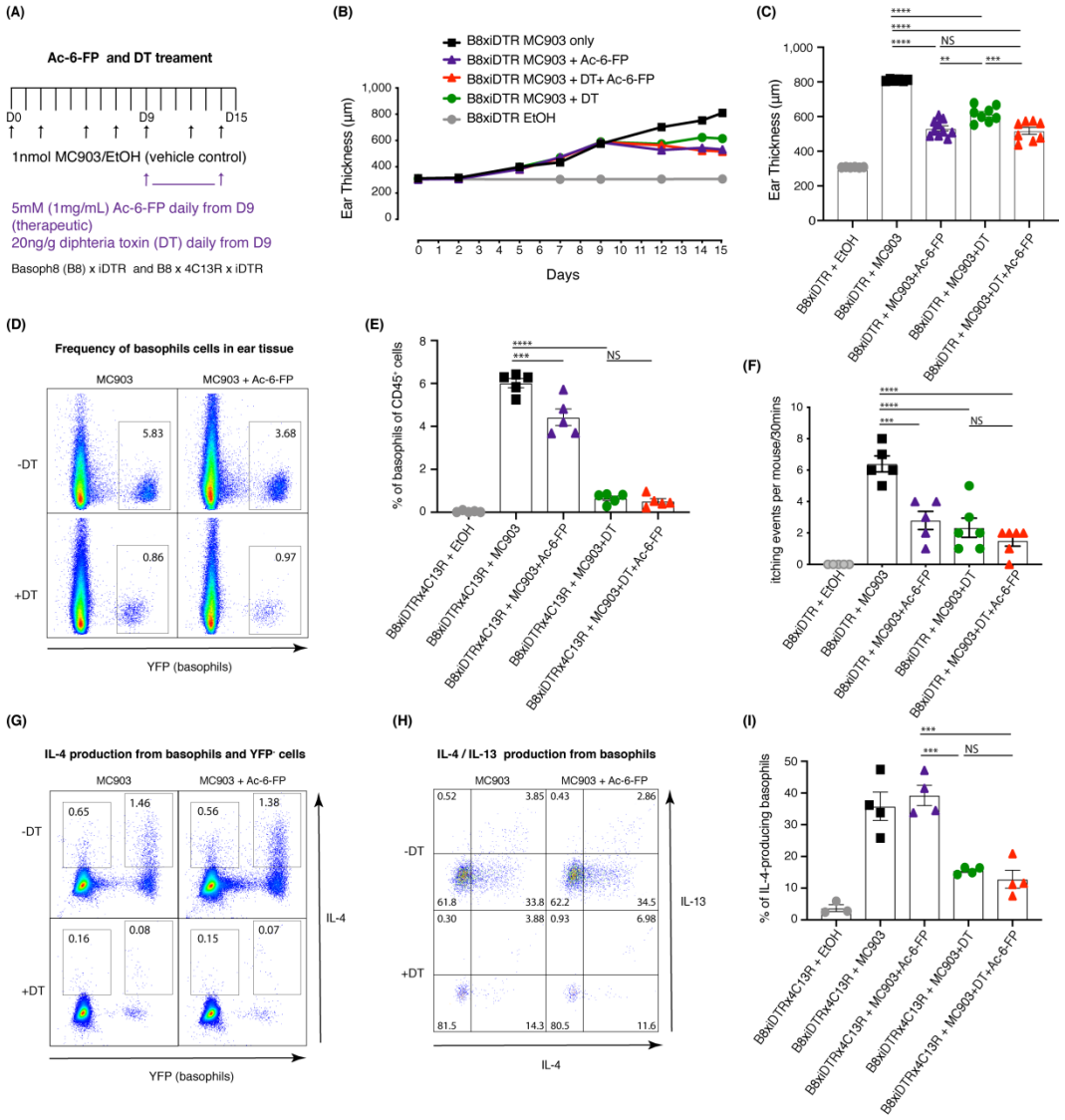


all_14994_f5.tif